Fermi Surface of Calcium by the de Haas–van Alphen Effect*

J. H. CONDON† AND J. A. MARCUS
Northwestern University,‡ Evanston, Illinois
(Received 26 November 1963)

The de Haas–van Alphen effect of calcium has been studied by the torsion method in fields to 33 kG. The three periodicities of 3.05, 0.77, and 0.57 (10^{-7}G^{-1}) that were observed had cyclotron masses of 0.3_5, 0.6_5, and $0.6_5 m_0$, respectively, and imply areas of orbits that are in agreement with a Few-OPW model with small lattice potentials, $V_{200}=0.034_5$ Ry and $V_{111}=0.01_4$ Ry. The experimentally-determined cyclotron masses are nearly twice those given by the model.

INTRODUCTION

THE availability of pure metals and large computers have made experimental and theoretical studies of the Fermi surface and band structure of metals very active fields in the past few years.[1] Of the experimental methods for the study of the Fermi surface, the torque method of the de Haas–van Alphen effect is applicable to metal samples of relatively less purity and needs only simple apparatus. The choice of a metal for study is still largely dictated by the availability of pure samples. In addition, calcium has some properties that make the study of its Fermi surface interesting. (1) The low melting point, luster, and ductility of calcium would lead one to suspect that it is a "simple" metal and can be well described by a nearly free-electron model. On the other hand, its proximity to the iron group elements might mean that the $4s$-$3d$ interaction is enough to make the Fermi surface significantly different from the nearly free-electron model.[2] (2) Calcium is a cubic metal and therefore the size and shape of the Fermi surface is simplified by symmetry. (In zinc, a hexagonal metal, the size of at least one section of the Fermi surface depends critically on the ratio of lattice parameters.[3]) (3) Calcium is valence two, and it is expected that the Fermi surface will contact the zone faces so that there will be a few small area orbits that can be studied by low-field de Haas–van Alphen effect.

Before proceeding to the main part of this paper, the sectioning of which is self-explanatory, we review for those acquainted with the field and introduce to others the de Haas–van Alphen (dHvA) effect and its relation to the Fermi surface.

The periodicity of the dHvA oscillations in $1/B$ gives those cross-sectional areas contained by the curves of intersection of the Fermi surface with planes perpendicular to **B**, i.e., electron or hole orbits, which are extremal with respect to variations of the position of the plane, by $A_m=2\pi e/\hbar cP$. A_m is in units of k^2, where $\hbar k$ is momentum and P is the periodicity in G^{-1}. This effect comes about because the action integral of the cyclotron motion is quantized and dependent on the magnetic field. As the magnetic field changes, the energy states pass through the Fermi energy and, since each state contributes to the magnetization in proportion to its population, the periodicity of the states crossing the Fermi energy creates a periodic magnetization.[4] The magnetization is not necessarily parallel to the applied field and therefore torques will exist in a sample in a uniform magnetic field. A complete theory[5] of the dHvA effect shows that the amplitude of the oscillations depends on the temperature and cyclotron mass approximately as $T\exp(-2\pi kT/\hbar\omega_c)$, where $\omega_c=eH/m_c c$. From measurements of the temperature dependence it is possible to find the cyclotron mass.

EXPERIMENTAL PROCEDURE

The dHvA oscillations in the torque are measured by a null deflection torsion balance of new design. The balance is a modification of a commercially available instrument, the Weston inductronic amplifier.[6] The electronics of the system are shown in Fig. 1; that part inside the dashed box is made by Weston and is supplied with the Inductronic galvanometer. Figure 2 shows the mechanical construction. The galvanometer structure was removed from the chassis and placed in a vacuum-tight case. Since the jeweled bearings supplied could not withstand the added load of the sample rod and sample they were removed and replaced by a torsion fiber made of Leeds and Northrup Std. 1114 0.002-in. 24K gold ribbon. The torque on the sample due to the magnetic field causes a rotation of the galvanometer coil E, so that some of the ~200-kc/sec alternating flux produced by coil F passes through the area of the galvanometer coil and a 200-kc/sec signal is induced across its terminals. This signal is amplified

* Part of a dissertation submitted to Northwestern University as required for the Ph.D.

† National Science Foundation Fellow and Cooperative Fellow 1960–1962. Present address: The Bell Telephone Laboratories, Murray Hill, New Jersey.

‡ Supported by the National Science Foundation and the Advanced Research Projects Agency of the U. S. Department of Defense.

[1] See, for instance, *The Fermi Surface* (John Wiley & Sons, Inc., New York, 1960).

[2] We thank L. Mattheiss [Phys. Rev. **133**, 1399 (1964)] for showing us the results of his band calculation for argon.

[3] W. A. Harrison, Phys. Rev. **118**, 1190 (1960).

[4] This treatment is carried out in detail in J. H. Condon, Ph.D. dissertation, Northwestern University, 1963 (unpublished) and gives the same results as the usual treatment (see Ref. 5).

[5] I. M. Lifshitz and Am. M. Kosevich, Zh. Eksperim. i Teor. Fiz. **29**, 730 (1955).

[6] R. W. Gilbert, AIEE Trans. **70**, 1121 (1951). Model 1411 is available from Weston Instrument Division, Newark, New Jersey.

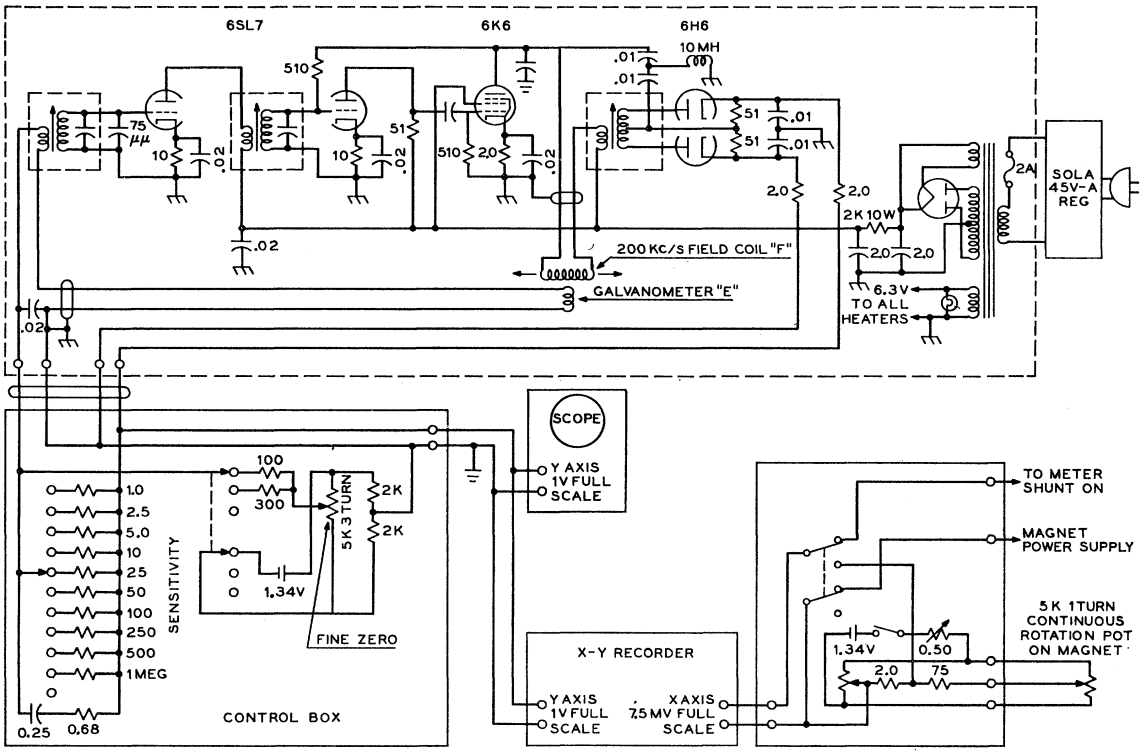

FIG. 1. Schematic diagram of the torsion balance and associated equipment. R in $10^3\,\Omega$, C in μf.

and added reactively to the oscillator circuit, thereby changing the oscillator frequency. A frequency discriminator produces a dc signal proportional to the frequency shift. This signal is recorded and fed back through the galvanometer coil to counteract the torque producing the original rotation. The capacitor and resistor shunting the sensitivity resistors provide damping for the system. The maximum practical sensitivity of the balance is 7.3 V/dyn-cm when the sensitivity resistor is $10^6\,\Omega$. The sensitivity may be decreased by a factor of 1000 by simply switching one resistor. The noise level of the system is always less than 10^{-3} dyn-cm and under ideal conditions may be less than 2×10^{-5} dyn-cm. The drift after one-hour warmup is less than 2×10^{-3} dyn-cm per hour and less than 15×10^{-3} dyn-cm per day when the instrument is operated from a constant voltage transformer.

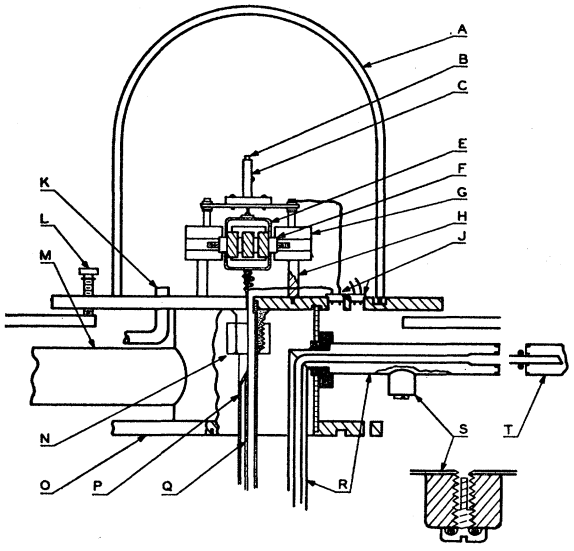

FIG. 2. Mechanical construction of torsion balance. A, bell jar; B and C, mount for upper suspension; E, galvanometer coil; F, 200-kc/sec field coil; G, soft iron pole pieces with powdered iron inserts; H, mounting studs; J, Kovar feed throughs; K, pump out and exchange gas inlet; L, leveling screws; M, pumping line for liquid He; N, modified compression fitting to mount; P, pyrex sample tube; Q, 1-mm quartz rod on which the sample is mounted; R, built in transfer tube; S, vacuum seal off operated by a "vacuum screwdriver" similar to Richard's; T, movable section of jointed transfer tube.

A rotatable A. D. Little Bitter iron core electromagnet, powered by a Cambridge Products Corporation power supply provides fields to 33 kG with <1 G uniformity and stability over the sample in a $\frac{7}{8}$-in. gap with 3-in.-diam pole caps. A common vacuum space liquid nitrogen shielded liquid helium Dewar flask, made by the H. S. Martin Company, pumped by a 30 cu. ft. per min. Kinney vacuum pump, provides temperatures down to 1.2°K. A magnet current shunt signal drives the X axis of the Mosely 2S recorder. The Y axis which records the torque is set at a sensitivity of 1 V full scale.

SAMPLE PREPARATION

High-purity calcium samples given to us by McCreary[7] with $(R_{300°}/R_{4.2°})=100$–300 were cut on a spark cutter

[7] W. J. McCreary, J. Metals **10**, 615 (1958).

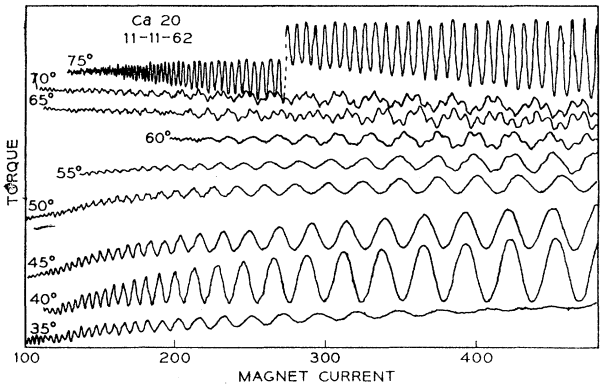

FIG. 3. Tracing of original data taken at 5° magnet angle intervals. The data for 75° was displaced upward midway to avoid overlap with that of 70°.

to reduce their size to about 3–5 mm on a side. The original samples, grown from vapor, show large faces that are all consistent with {110} type planes, and the samples were oriented by the faces. Since the dHvA effect is a bulk effect, no stringent precautions were taken about retarding surface contamination. After an exposure of about an hour to air, a tough black film appears on the surface which seems to retard the formation of the white oxide, however the oxide will form rapidly in humid air. These surface contaminations destroy the x-ray back reflection patterns, and were removed by treatment with either HCl or HNO_3 diluted in either dry acetone or absolute alcohol.

EXPERIMENTAL RESULTS

A sample of the data, redrawn for reproduction, is shown in Fig. 3. In this experiment the temperature was 1.3°K and the magnetic field swept from ~21 to ~33 kG. The largest peak to peak torques shown by the different curves which were taken at five-degree intervals of magnet angle is about one-tenth dyn-cm.

To reduce the data we count a number of oscillations and, by means of a calibration curve made previously

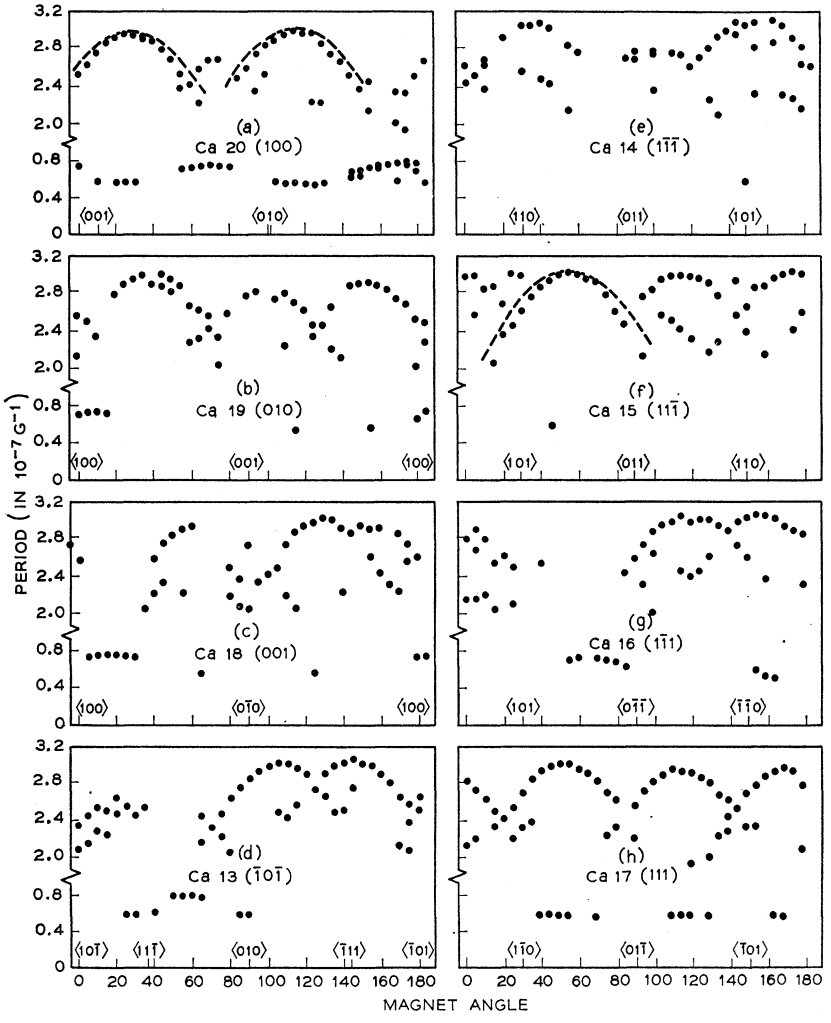

FIG. 4. Observed periods as a function of applied field direction. Dashed curves are $3.05\cos(\theta+\phi)$ with ϕ adjusted for best fit.

with a NMR probe-frequency counter combination, find the difference in $1/H$ between the two ends of the counted range. Figure 4 shows reduced periods as a function of orientation given by this method on one sample for different planes of rotation of the magnetic field. The notation of the crystal directions does not assume equivalence of axes. The [100] direction is the growth direction of the sample. The other two axes are named consistently with the crystal's growth faces.

The data of Fig. 4 do not show the expected symmetry except in two cases, Fig. 4(a) and Fig. 4(h). However, here the symmetry directions of the data are badly out of line with the symmetry directions according to the morphology. These data are typical of data from several other samples with the exception that the data from samples which had smaller growth faces do not suggest the smooth curves in the period versus magnet orientation plots that these data do. It is concluded that no samples are single crystals and that the samples with smaller growth faces are more polycrystalline. The x-ray back reflection photograph of the sample of Fig. 4 shows a number of large spots with no symmetrical pattern and indicates strain, only one very faint line of spots was visible. The fact that there is a suggestion of smooth curves in Fig. 4 for the longest period indicates that the sample must contain only a few larger grains that dominate over the rest of the sample. The polycrystalline nature of the sample makes any interpretation of the crystallographic directions at which the periods are observed, as determined by Fig. 4, very doubtful. However, there are three points that are apparent from data shown in Fig. 4.

(1) Three distinct orbits on the Fermi surface are observed with maximum periods of $3.05\times10^{-7}G^{-1}$, $0.77\times10^{-7}G^{-1}$, and $0.57\times10^{-7}G^{-1}$. Figure 5 shows histograms of the number of observances of each period. All the data of Fig. 4 are replotted here. The experimental error in the periods can be judged from these histograms. The error due to errors of magnetic-field calibration is smaller than the uncertainty of choosing the maximum periods, which we judge to be 2, 5, and 5% for the three periods.

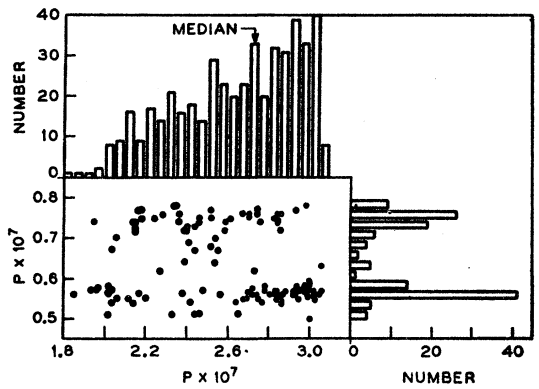

FIG. 5. Histograms of the number of observations of each period and correlation plot of simultaneous observations of a long and short period.

(2) The longest period is due to a piece of the Fermi surface which is "hyperboloidal." This is seen in Figs. 4(a) and 4(f) where a cosine curve is plotted for comparison; as the magnetic field is rotated away from the angle at which the period is a maximum, the period decreases more rapidly than the cosine curve. This implies that the area of the orbit is increasing more rapidly than an orbit due to a cylindrical piece of Fermi surface.

(3) There is a correlation between the observation of the shortest period and the observation of the longest period. Likewise, there is a negative correlation between the longest period and the 0.77 period. This is shown by the correlation plot of Fig. 5. At each orientation where a short and long period are simultaneously observed a point is plotted. If only one period is observed no point is placed. If more than one long period and/or more than one short period are observed at any orientation a point is plotted for each of the possible pairs of coordinates. Only 25% of the points in the region about 0.77 are above the median of the histogram of the 3.05 period, which implies strong negative correlation. 65% of the points in the region about 0.57 are above the median, implying a weaker positive correlation. If the sample contained a large number of randomly oriented grains we would expect to see no correlation of this type and, therefore, the correlation substantiates the hypothesis that the behavior of the sample is dominated by only a few crystallites. Also the fact that any correlation is observed in this sample implies that the correlation would be much higher in a single crystal sample, and so we believe that even these weak correlations of observations are important.

In addition to the information from the data of Fig. 4, the cyclotron masses have been determined from the temperature dependence of the amplitude of the oscillations. The longest period, 3.05, has a cyclotron mass of $0.35\pm10\%\, m_0$. Due to the extreme angular dependence of amplitude, the precision of the mass determinations of the short periods is limited by the reproducibility of magnet angle settings for the experiments at different temperatures. Furthermore, the amplitudes of the shorter oscillations were only sufficiently large to measure accurately when the temperature was less than $\sim2.5°K$ and so limited the range of study. We selected data of large amplitude and small angular dependence and found the average of eight determinations of the mass of the 0.77 period to be $m_c=0.62\pm15\%\, m_0$. The average of seven determinations for the 0.57 period is $m_c=0.65\pm15\%\, m_0$.

We were not able to determine the Dingle scattering factor because the mixture of several very close periods made it extremely difficult to estimate the magnetic field dependence of the amplitude.

The shortest period and its cyclotron mass agree very

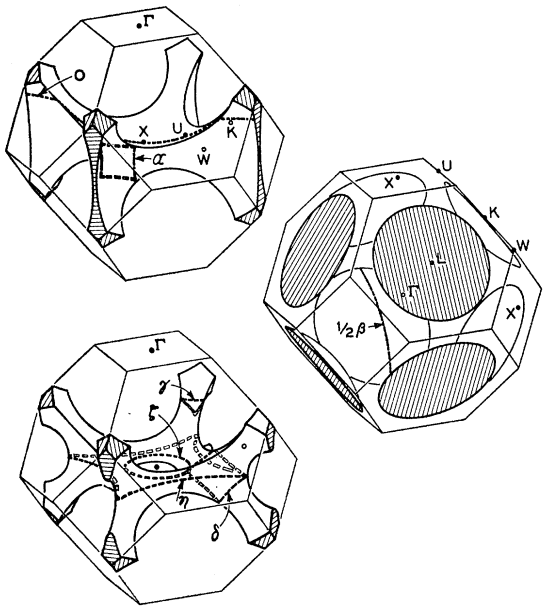

FIG. 6. Fermi surfaces for calcium. Upper left, first-zone holes, single-OPW; Right, second-zone electrons, single-OPW and few-OPW; Lower left, first zone, few-OPW; $V_{200}=0.05E_F$, $V_{111}\simeq 0$. Orbit α also exists in the few-OPW first band but is omitted for clarity. Orbit 0 is an open orbit in the first zone which exists only for very small V_{200}.

well with Berlincourt's[8] determination of $P=0.59\pm 10\%$ $\times 10^{-7}\mathrm{G}^{-1}$ and $m_c=0.61\pm 10\%\, m_0$ by the impulsive field technique. Since his samples were from the same source as ours, we feel that they too are probably not single crystals and that, as with our data, the direction of applied field (i.e., [100]) should not be given much weight in interpretation.

The discrepancy of our previous report[9] of a period of $2.9\times 10^{-7}\mathrm{G}^{-1}$ and the present value, $3.05\times 10^{-7}\mathrm{G}^{-1}$, can be explained by the amplitude dependence on period found in the more recent experiments, which is maximum when the period is 2.8–2.9. We believe that in the old experiments at lower fields we were able to observe the oscillations only when the amplitude was largest.

The experimental results are reviewed in the first half of Table I.

INTERPRETATION OF DATA

Even though the data lack the symmetry one would expect from a single crystal and the dependence of period on magnetic field direction relative to the crystal axes is not available for use, there are dHvA oscillations present and the experimental data must be explainable by some model of the Fermi surface. Since there is reason to believe that the Fermi surface of calcium will be described well by a single-OPW or few-OPW model with small lattice potentials, comparison will only be made to these models.

TABLE I. Experimental results and comparison to model.

Experimental data				
Period ($10^{-7}\mathrm{G}^{-1}$)	m_c/m_0	Correlation[a]	Shape	$\frac{m_c(\text{exp.})}{m_c(\text{theo.})}$
3.05±2%	0.30±10%	···	hyper.	1.9±10% (γ)
0.77±5%	0.62±15%	strong−	?	2.1±15% (α)
0.57±5%	0.65±15%	weak+	?	2.1±15% (β) or 1.9±15% (δ)

Theoretical model					
Orbit	Period[b]	Period[c]	m_c/m_0[b]	Correlation[a]	Shape
γ	2.85	2.90–3.10	0.16	···	hyper.
α	0.72	0.74–0.75	0.30	strong−	hyper.
β	0.56	0.55–0.56	0.31	weak+	ellipsoid
δ	0.55	0.55–0.56	0.35	strong+	hyper.

[a] Correlation of observation with the 3.05 period as under "Experimental Results."
[b] $V_{200}=0.13$, $V_{111}=0.01$; Harrison's values (Ref. 9).
[c] $V_{200}=0.095$–0.100, $V_{111}=0.04$; "Best values" of this work.

The single-OPW construction published by Harrison[3] is shown in Fig. 6. There are two orbits, the periods of which are approximately those given by experiment. Orbit α in the first band would give a period of $0.77\times 10^{-7}\mathrm{G}^{-1}$ and orbit β in the second band would give a period of $0.48\times 10^{-7}\mathrm{G}^{-1}$. Considering that α will be observed with H applied nearly along a ⟨100⟩ direction, and β will be observed with H nearly in a {111} plane, and the correlation of observation noted in the previous section, we attribute experimental period 0.77 to the orbit α and the period 0.57 to the orbit β. However, there is no orbit which corresponds to the longest period 3.05.

The thickness of the Fermi surface structure at the point X is $\sim 3\%$ of the distance ΓX; therefore a lattice potential V_{200} that is $>3\%$ of the Fermi energy would pull the Fermi surface to the ⟨200⟩ faces near X. Harrison[10] has calculated the lattice potentials to be $V_{111}=0.003\,\mathrm{Ry}\simeq 0.9\%\, E_F$ and $V_{200}=0.039\,\mathrm{Ry}\simeq 12\%\, E_F$ and so contact is very likely. In this case (Fig. 6) new orbits will appear; orbit η will have too large an area to explain any of the experimentally-observed periods. Orbit ζ lies in a zone face and will have, according to a 2-OPW model, a cyclotron mass equal to m_0; furthermore, it will exist only with H applied very close to a ⟨100⟩ direction. It is unlikely that this orbit can explain any of the periods observed experimentally. Orbit δ may have a period which corresponds to the shortest period observed, 0.57, depending on the exact values of the lattice potentials V_{111} and V_{200}. It should be observed with H applied nearly in a ⟨110⟩ direction. This is consistent with the correlations of observations and the 0.57 period may be attributed to the orbit δ as well as to the orbit β. The orbit γ has a small area

[8] T. Berlincourt, *Proceedings of the Seventh International Conference on Low-Temperature Physics* (The University of Toronto Press, Toronto, 1960), p. 231.
[9] J. H. Condon and J. A. Marcus, Bull. Am. Phys. Soc. **6**, 145 (1961).
[10] W. A. Harrison, Phys. Rev. **131**, 2433 (1963).

and with proper choice of lattice potentials, can explain the longest observed period. Oscillations due to orbit γ will be observed when H is nearly along a $\langle 110 \rangle$ direction. The Fermi surface is hyperboloidal in shape here and all the experimental observations check with the model as we make the assignment $\alpha \leftrightarrow 0.77$, β or $\delta \leftrightarrow 0.57$, and $\gamma \leftrightarrow 3.05$.

We now proceed to a quantitative description of the Fermi surface for comparison to our experimental results. The shape of constant energy surfaces near a zone face may be described quite accurately by a 2-OPW model. Except near the junction of two or more faces the inclusions of more OPW's into the model makes only a perturbation of the energy. In regions far from all zone faces the constant energy surfaces are spherical, or free-electron like.[11] Figure 6 shows that the single-OPW Fermi surface does not come very close to the junction of zone faces and we can confidently propose a model of the Fermi surface the shape of which is given by appropriate 2-OPW models near the square and hexagonal faces and by a spherical section joining them. The energies used in the 2-OPW and spherical segments are not equal but must be adjusted so that the segments join up smoothly and so that the surface contains the right volume for a valence two material, i.e., a volume equal to the zone volume. This last point turns out to be very important in calcium. The effect of the lattice potential V_{111} on the volume of a constant energy surface is small since the volume increase of the electron surface in the first band is largely cancelled by

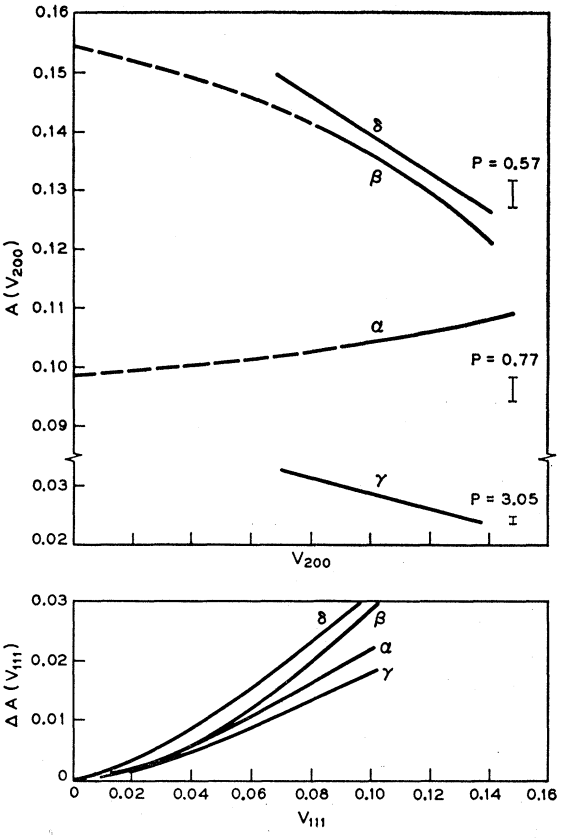

FIG. 8. $A'(V_{200})$ and $\Delta A(V_{111})$. A' and ΔA in $(2\pi/a)^2$, V_{200} and V_{111} in $\hbar^2/2m_0a^2$. See text.

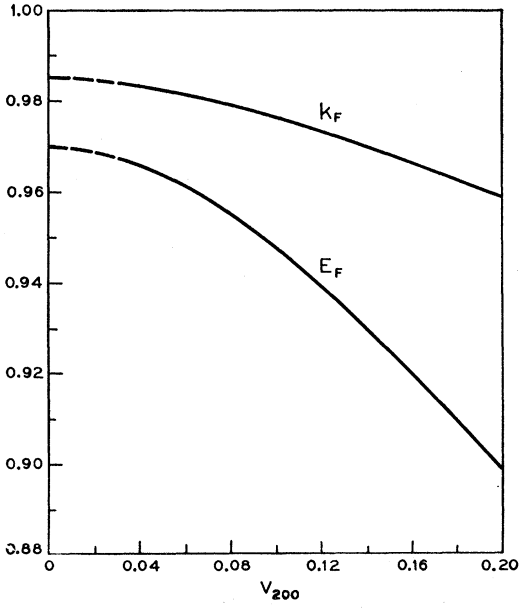

FIG. 7. E_F and k_F as functions of V_{200} computed such that the volume of the Fermi surface equals the volume of the zone and the Fermi surface is smooth. E_F and V_{200} are in units of $\hbar^2/2m_0a^2$, k_F is in units of $2\pi/a$.

[11] M. H. Cohen and V. Heine, Advan. Phys. **7**, 395 (1958).

the volume decrease in the second band, but the effect of increasing V_{200} is considerable. There is no segment in the second band that has a volume decrease of the same order as the volume increase of the constant energy surface in the first band as it is drawn to the symmetry point X and contact spreads circularly outward. Since the volume of the Fermi surface must remain constant we expect a decrease in the Fermi energy with increasing V_{200}. To calculate $E_F(V_{200})$ we consider a valence one simple cubic metal since the effect of V_{111} is of no importance. The Fermi surface will be spherical with six "suction cups" on it in the $\langle 100 \rangle$ directions. The shape of each cup is given by a 2-OPW formula and the energies of the 2-OPW model and sphere are adjusted so that they join smoothly as the $\{\frac{1}{2},0,0\}$ planes. The volume of this surface is easily calculated by integration and may be adjusted to the correct volume by a rapidly converging iteration procedure by adjusting the Fermi energy in the 2-OPW formula and radius of the sphere. The Fermi energy and radius of the sphere are shown in Fig. 7 and show the rapid decrease of E_F with increasing V_{200} as expected.

To calculate the areas of orbits we make a further simplification, namely, the area of any orbit can be expressed as

$$A_n(V_{200},V_{111})=A_n'(V_{200})-\Delta A_n(V_{111}). \quad (1)$$

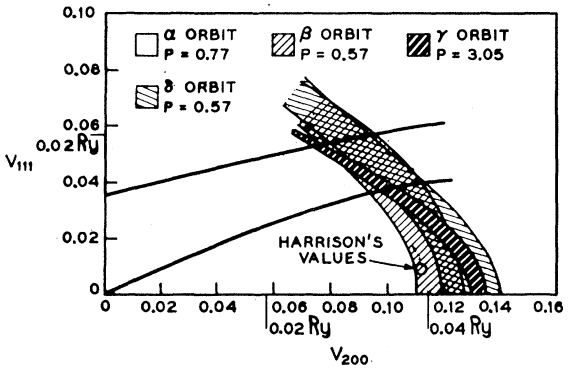

FIG. 9. Allowed regions on the V_{200}–V_{111} plane, V in $h^2/2m_0a^2$ and in rydbergs.

Figure 8 shows $A_n'(V_{200})$ as determined by drawing cross sections of the 2-OPW model with $E=E(V_{200})$ and sphere with $k_F=k_F(V_{200})$ as already determined and measuring the areas with a planimeter, and also shows $\Delta A_n(V_{111})$ as estimated by analytic integration. At the right edge of the graph are shown the areas that correspond to the experimentally-observed periods. The periods predicted by the areas calculated by Eq. (1) using Harrison's values of V_{200} and V_{111} and the results in Fig. 8 are shown in the table. Rather than compare the theoretical predictions to the experimental results, we see that if the $A(V_{200},V_{111})$ of Eq. (1) is limited to the experimentally-determined areas including error, this restricts V_{200} and V_{111} to a band on the V_{111}, V_{200} plane. These bands are shown in Fig. 9. From this we conclude that the "best values" of the lattice potentials are $V_{200}=0.0345\pm0.001$ Ry and $V_{111}=0.014\pm0.002$ Ry. The periods predicted by these values are also shown in the Table for comparison to the experimental results.

Figure 9 implies two interesting points. The first is that even if we were given the values of V_{200} and V_{111} we could not decide whether the 0.57 period should be attributed to orbit β or orbit δ. Second, if the band due to the orbit α were not included there would be a large range of values of V_{200} and V_{111} consistent with the other experimental results. In this case, even if the theoretical periods and experimental periods agree, one could not conclude that the calculated lattice potentials were correct.

Throughout the lattice potentials have been taken to be momentum-independent. Since the shape of the Fermi surface is not critically dependent on the lattice potentials except near the zone faces we expect the momentum-independent approximation to be very good. Furthermore, the dHvA effect is not sensitive to such fine details.

The masses given in the table for the orbits α and β are those of the single-OPW model but the masses of the few-OPW model are not significantly different. The orbits δ and γ do not exist in the single-OPW model and the masses given have been calculated by planimeter integration around the orbit using a few-OPW model with Harrison's values of lattice potentials, but the masses do not change significantly for our values. Also shown in the Table is the ratio of the experimentally observed masses to those predicted. The ratio is ~2 for all the orbits. This factor of two has been noted before[3] in Pb and Al.

On reinspecting it appears that there is no way to decide if the shortest period observed should be attributed to orbit β or orbit γ. Either is consistent in area and cyclotron mass. The magnitude of the correlation of observation is too uncertain to decide. In all probability some observations are due to β and some to γ.

It is now possible to predict the periods of other orbits that might be observable in future experiments. The orbit ζ will have a period of $0.51\times10^{-7}\text{G}^{-1}$ and if the "factor of two" occurs for this orbit the observed cyclotron mass will be $\sim2m_0$. The orbit around the edge of the lens in the second band will produce a period $\sim9.6\times10^{-9}\text{G}^{-1}$ with $m_c\simeq2m_0$ and, finally, the orbit η will have $P\sim8.6\times10^{-9}\text{G}^{-1}$ and $m_c\simeq2m_0$.

In Fig. 6 there is shown a possible open orbit. This open orbit disappears as the contact of the Fermi surface with the {200} zone faces increases in size. We believe the contact to be large enough to preclude any such open orbits and expect the magnetoresistance to be quadratic everywhere.

CONCLUSIONS

We have shown that de Haas–van Alphen data of polycrystalline calcium is consistent with a few-OPW model with lattice potentials not very different from Harrison's calculated potentials. The polycrystalline nature of the samples makes the data too inaccurate for any comparisons of detailed differences between a complete band calculation and a few-OPW calculation. Study of a single-crystal sample will certainly clear up a number of the difficulties in the present work.

ACKNOWLEDGMENTS

We acknowledge W. A. Harrison for reminding us of the existence of orbit α and making available to us the results of his calculations and T. Berlincourt for providing us with the first sample of calcium and referring us to W. J. McCreary to whom we are indebted for other samples.

Finally we thank many others too numerous to name who helped in the experiments and interpretation of the results.